TTMP vol 1(3), 2024
doi: 1030511/TTMP.2024.2037356.1036

Transactions in Theoretical and Mathematical Physics

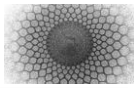

Modeling and investigation of double-layer InP/AlGaInP quantum dot lasers based on dot size*

Mohammad Reza Mansouri[a,1], Tahere Zare[2], Sara Jafakesh[3]

[1] Department of Electrical Engineering, Lamerd Branch, Islamic Azad University, Lamerd, Iran
[2] Department of Mathematics, Beyza Branch, Islamic Azad University, Beyza, Iran
[3] Department of Electrical Engineering, Lamerd Branch, Islamic Azad University, Lamerd, Iran

Received: 02 August 2024 / Accepted: 19 August 2024 / Published: 25 August 2024

Abstract This paper investigates the spectrum theory of a self-aligned InP/AlGaInP bilayer quantum dot laser fabricated by organic-metallic vapour phase epitaxy. The dipole size distribution of quantum dots (groups of small and large quantum dots) has been identified in the fabrication process. Therefore, a model based on song equations that considers the superposition of two heterogeneous groups of quantum dots has been proposed. The total output power and power spectral density (PSD) of the fabricated quantum dot laser at room temperature are determined theoretically. Also, the output spectrum is divided into the sum of two Gaussian (super-Gaussian) curves corresponding to the groups of small and large quantum dots. Each group's peak power spectral density (PSD) and spectral width are extracted, and their dependence on the injection current density is investigated. The results show that the peak corresponding to large quantum dots dominates at low currents, while at high currents, the peak corresponding to small quantum dots dominates, and its spectral width decreases. This behaviour is attributed to the saturation of energy levels of large quantum dots due to their relatively long radiative lifetimes.

1 Introduction

The emergence of quantum dot (QD) lasers in the late 80s marked a revolution in optics and photonics and attracted the attention of scientists in universities and industries. The inherent advantages of these lasers over traditional quantum well lasers have made them ideal options for a wide range of applications. The key feature of many of these lasers that distinguishes them from other lasers is the low threshold current that causes them to require less energy to start operation, resulting in better consumption and higher efficiency [1]. Discrete energy levels cause the electrons to be trapped in these discrete levels and increase the performance and stability of the laser significantly [2]. They work more effectively at higher temperatures than quantum well lasers, making them more suitable for challenging applications and high-pressure environments [3]. Another feature of these lasers is the narrow emission lines that cause them to emit light with a very precise wavelength and produce a purer colour with a broader bandwidth [4]. Significant progress in the growth of self-organizing nanostructures with small sizes is the turning point of these lasers, which enables the production of lasers with arbitrary wavelengths [5]. This spectral performance enables high-bandwidth data transmission with visible light, revolutionizing next-generation communications. Another feature of QD lasers is their higher precision and sensitivity in making optical sensors that can be used in medical, military, and measurement imaging applications. Temperatures are used [6] and are also a key component for the development of quantum computers and other quantum technologies in the future [7]. Red-wavelength quantum dot (QD) lasers made of InP implanted on a GaInP base have a dual dot size distribution (small and large quantum dots) [8]. This effect is related to the roughness angle of the substrate and different growth conditions such as surface diffusion, growth temperature, and growth rate. Due to the limitations of the jump between the barrier band and the energy levels, the expected stability threshold of the laser decreases with increasing temperature. As a result, aluminium (Al) is added to the barrier material to reduce the possibility of thermal escape of charge carriers and, as a result, confinement of point charge carriers. Quantum increases [9]. The amount of aluminium is adjusted according to what was suggested in [10] to reach the optimum composition of InP implanted in the (Al0.1Ga)0.51InP barrier [11]. Although the difference between the ground state and the first excited state is small, 13 nm, the gain is nevertheless limited by the low dot density and poor optical confinement factor. To overcome this challenge, a solution based on the vertical arrangement of QD layers has been proposed, which offers several advantages, including higher gain [12], the possibility of ground state emission, and a higher gain saturation limit [13]. By increasing the number of stacked layers, a shift towards red wavelengths is observed in the laser [14]. In addition, overlapping layers lead to increased external efficiency [15]. In [16], two InP layers in (Al0.1Ga)0.51InP barriers with a spacer thickness of 6 nm have been achieved with a pure mode efficiency of 68.5% compared to 43.7% for a single layer [17], and the change in wavelength between the peaks The two groups of QDs

[a]e-mail: mansouri1902@gmail.com

(small and large) are about 45 nm. Therefore, modelling these important effects using song equations is necessary to fully understand the optical properties of lasers. This paper presents a theoretical model based on experimental data for InP/(Al0.1Ga)0.51InP double-layer quantum dot lasers with a 4 nm spacer fabricated by metal-organic vapor phase epitaxy [18]. The proposed model is based on the song equations and considering the combination of two heterogeneous groups of quantum dots (small and large) that are formed during the construction, the output spectrum is divided into the sum of two Gaussian curves belonging to the small and large QD groups. The peak power spectral density (PSD) and spectral width of each group in the output spectrum are extracted, and their dependence on the injection current density is analyzed. This model is the first model for the binary size distribution of QD InP laser systems. The organization of the structure of this article includes an introduction of the QD multi-mode rate equation model, an experimental model, a discussion about theoretical results, and comparison with the experimental model, and a conclusion.

2 Modeling of the rate equation

This model is based on considering two types of heterogeneity in the system. The first type is the inhomogeneity between small and large groups of quantum dots, which was observed in the atomic force microscope (AFM) images in sources [19] and [20]. The second type is heterogeneity within each group due to size variations around the standard QD size. It is assumed that all quantum dots are spatially separated and the two QD layers do not interfere with each other so that the output of the laser system is the sum of their outputs. The presence of two layers results in a larger number of QDs and, consequently, a higher gain. The neutrality of the QD is maintained by trapping only electron-hole pairs with equal lifetimes. The principle of Pauli exclusion and spin degeneracy is respected in the calculations. The system's operation starts with injecting pulsed current source carriers into the coating layer. The carriers then move to the active region, releasing them from the barrier through the wet layer. Finally, the carriers are trapped at the highest energy level inside each QD and can then escape to lower energy levels. The number of energy levels and their energy separation depends on the QD size. For example, a large QD has multiple energy levels with little energy difference. On the contrary, the small size of the QD leads to a smaller number of energy levels with a greater distance between them. The presented model assumes that all the carriers injected by the pulsed current source reach the wet layer, the lowest energy level, and the ground state inside each QD is considered. The energy level of the wet layer (E2) and the ground state energy levels of the two QD groups are ($E1^S$, and $E1^L$), referring to the small and large groups; the wet layer collects carriers with an average injection rate that is similar to the effective current of the pulsed current source. When the carrier reaches the ground state, carrier-photon interactions occur through the gain-excited process (gm^S, gm^L). The numerical model is based on the solution of the photon-carrier rate equations in the framework of the model of the main equations of carrier dynamics. Fig. 1 shows the proposed model.

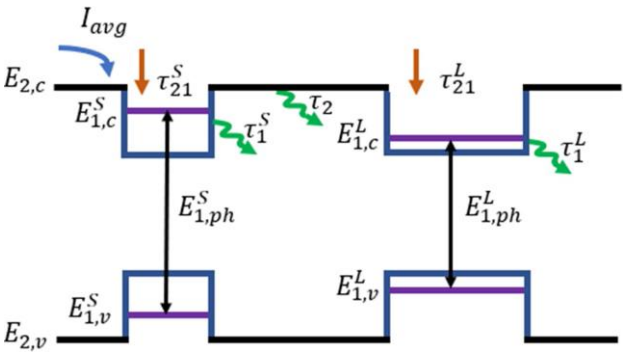

Figure 1 Carrier dynamics model with energy levels and wet layer of quantum dot laser.

The propagation equations of the input signal take an exponential form in each section to amplify the signal through the cavity length, which is as follows. For more details on equations and the introduction of parameters, see [15]. Therefore, the numerical solution of the rate equations with the fourth-order Runge–Kutta method is used in each section for all cavity modes to evaluate the spectrum in the QD laser. rate equations are solved numerically in this section with MATLAB software, and ode45 code was used for this analysis. Some parameters used in the calculations are listed in Tab. 1.

Table 1 Parameters which are used in the calculation and simulation

Parameter	Symbol	Value
Active region length	$[L]$	1200 μm
Active region width	$[W]$	1.50 μm
Band gap	$[Eg]$	0.08eV
Central transition energy of GS	$[Ej]$	0.9493eV
Central transition energy of ES1	$[Em]$	1.0221eV
Number of QDs layers	$[Nl]$	10
Optical confinement factor	$[\Gamma]$	0.1
Carrier recombination lifetimes in dots	$[\tau r]$	1ns
Carrier recombination lifetimes in WL	$[\tau \omega r]$	0.4ns
Temperature	$[T]$	295K

$$\frac{dN_2}{dt} = \frac{I_{avg}}{e} - N_2 \sum_L^{N_L} \frac{(1-f_1^l)G^L}{\tau_{21}^L} - N_2 \sum_S^{N_S} \frac{(1-f_1^S)G^S}{\tau_{21}^S} - \frac{N_2}{\tau_2} + \sum_L^{N_L} \frac{(1-f_2^L)N_1^L}{\tau_{21}^L} + \sum_S^{N_S} \frac{(1-f_1^S)N_1^S}{\tau_{12}^S} \quad (1)$$

$$\frac{dN_1^L}{dt} = \frac{N_2 G^L}{\tau_{21}^L}(1-f_1^L) - \frac{N_1^L}{\tau_1^L} - \frac{(1-f_2^L)N_1^L}{\tau_{12}^L} - \Gamma_L \sum_m^{N_m} g_{m,1}^L v_g S_m \quad (2)$$

$$\frac{dN_1^S}{dt} = \frac{N_2 G^S}{\tau_{21}^S}(1-f_1^S) - \frac{N_1^S}{\tau_1^S} - \frac{(1-f_2^S)N_1^S}{\tau_{12}^S} - \Gamma_S \sum_m^{N_m} g_{m,1}^S v_g S_m \quad (3)$$

$$\frac{dS_m}{dt} = \Gamma_L \sum_L^{N_L} g_{m,1}^L v_g S_m - \Gamma_S \sum_S^{N_S} g_{m,1}^S v_g S_m + \beta_L \sum_L^{N_L} \frac{N_1^L}{\tau_1^L} + \beta_S \sum_S^{N_S} \frac{N_1^S}{\tau_1^S} - \frac{S_m}{\tau_{ph}} \quad (4)$$

τ_{ph} is the photon lifetime in the cavity. The overall optical gain is given by the following equation:

$$g'_{m,L} = \frac{2\pi e^2 \hbar < R_{eh} > N_{QD}^j}{c n_r \varepsilon_o m_o^2} \left(f_{L,c}^j - f_{L,o}^j\right) G^j\left(E_j - E_j^o\right) \times (E_m - E_j) \quad (5)$$

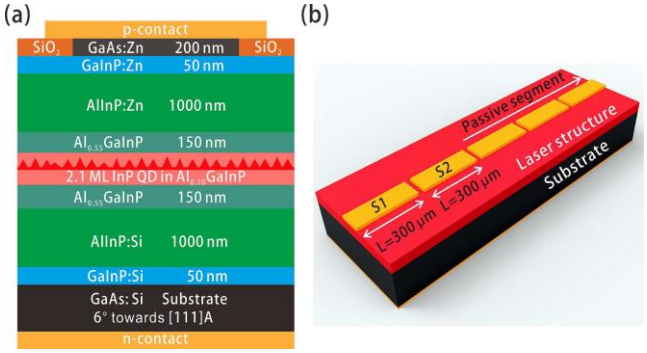

Figure 3 Schematic drawing of the test structures (not to scale): (a) Epitaxial layers designed for a 660 nm emitting InP/AlGaInP QD broad area laser. (b) Measured structure of the optical gain and absorption spectra with segmented contact sections. S1: segment 1, S2: segment 2, Passive segments: the long enough segment sections to avoid the reflected light.

The homogeneous broadening of the induced emission process with the Lorentzian function is given as follows.

$$B_{cv,j}(E_m - E_j) = \frac{\hbar\,\Gamma_{cv,j}/\pi}{(E_m - E_j)^2 + (\hbar\Gamma_{cv,j})^2} \quad (6)$$

$\hbar\Gamma_{cv,j}$ is the FWHM (full width at half maximum) of the homogeneous broadening in each energy state. The inhomogeneous spread with Gaussian distribution function is given below:

$$G^j(E_j - E_j^o) = \frac{1}{\sqrt{2\pi}\varepsilon_o} exp\left[-(E_j - E_j^o)^2/2\xi_o^2\right] \quad (7)$$

3 Experimental model

The investigated QD laser structure was grown by metal-organic vapour-phase epitaxy (MOVPE) on a Si-doped (100)-GaAs substrate with a misorientation of 6^0 toward the $[111]_A$ direction. An AIX-200 horizontal reactor was used for the epitaxial growth with standard precursors (trimethylgallium, trimethylindium, trimethylaluminium, arsine, and phosphine), at a high temperature of 710^0 C and a reactor pressure of 100 mbar to achieve a high density of QDs. As shown in Fig. 2(a), from bottom to top, the laser structure consists of a 100-nm-thick GaAs: Si buffer layer, followed by a 50-nm-thick Ga 0.52 In 0.48 P: Si intermediate layer and a 1000-nm thick Al0.52 In 0.48 P: Si optical confinement layer (OCL). Afterwards, a single sheet of 2.1 monolayers (ML) self-assembled InP QDs were grown in the Stranski-Krastanow (S-K) mode and placed in the centre of the 2 × 10 nm undoped Al0.10 GaInP barriers. The barrier layers were carefully adapted to be lattice-matched to GaAs. The entire active region was surrounded by 2 × 150 nm undoped Al0.55 GaInP waveguide layers to form the separated confinement structure (SCH) and get the highest optical confinement factor in the vertical direction. The p-side has a structure similar to the n-side, while the dopant was changed to zinc. The layers were finally capped by a 200-nm-thick heavily doped GaAs: Zn layer to form an ohmic contact with low resistance. For the processing of broad-area lasers, a 100-µm-wide stripe contact layer of GaAs: Zn was first formed by photolithography and wet chemical etching to reduce the current spreading in the lateral direction. After depositing a SiO_2 insulation layer, Pd/Au layers were metalized on top to form the p contact. To reduce the thermal effect, the substrate was polished down to about 130 µm, followed by depositing the Cr/Au-based n-contact on the substrate backside. Afterwards, the sample was processed into the Fabry-Perot (FP) lasers by cleaving the facets with different cavity lengths between 0.55 and 2.24 mm.

The segmented contact method described in [21] was utilized to measure the optical gain and absorption spectra by analyzing the amplified spontaneous emission (ASE) as a function of the contact stripe length. To implement this method, the p-contact of the gain-tested sample, as represented in Fig. 2(b), was separated into 300-µm-long segments with a gap of 5 µm in between, while the segment width remained 100 µm. All the cleaved facets of the test samples were uncoated. The samples were measured on the brass heatsink controlled by a temperature controller, and the current application was done using an Au-coated tungsten probe. The measurements were operated under the pulsed current driven with a duration of 300 ns and a duty cycle of 0.15% to avoid the self-heating effect.

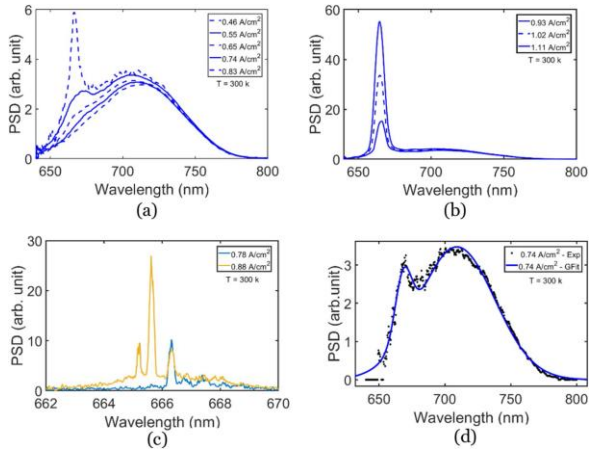

Figure 4 PSD versus wavelength for different current densities.

This section presents the results of the experimental study on the InP/AlGaInP bilayer quantum dot laser chip at room temperature. These results are taken from [15] and [21]. Fig. 3 shows the relationship between the average output power of the InP/AlGaInP bilayer quantum dot laser and the average injected current density for three different duty cycles (0.075%, 0.1% and 0.15%) at room temperature. Fig. 4 shows the laser output spectrum for different average injection current densities and duty cycle of 0.1%. The resolution of the spectrometer analyzer is set to 50 picometers in figs (c4) and 2 nm for the other figures. Also, the information extracted from Gaussian fitting for groups of small and large quantum dots against the average current density is shown in Figs (5a) and (5b). These observations can be explained as follows. In the first region, where large quantum dots dominate the spectrum, the small energy separation of the excited states for the group of quantum dots facilitates carriers' transition from the wet layer to the ground state in a shorter time than for small quantum dots. However, in the second and third regions, as shown in Fig. 3a, small quantum dots dominate and emit lasers, while large quantum dots are saturated. This is due to the higher mode gain of small quantum dots compared to larger dots [22]. Even at low injected current density, the luminescence of large quantum dots saturates, and the overall spectrum shifts to shorter wavelengths (Fig. 4a). This behavior is due to the filling of the ground state due to the weak overlap of wave functions between electrons and holes, which leads to long lifetimes of charge carriers. Charge carriers in small quantum dots show a stronger overlap of wave functions and therefore recombine much faster, leading to Higher emission intensities in higher energy spectral range.

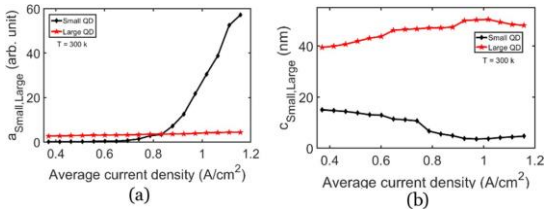

Figure 5 Data extraction for small and large QD groups from Gaussian fitting versus average current density. a. The peak amplitude of the Gaussian PSD. b. Gaussian spectral width.

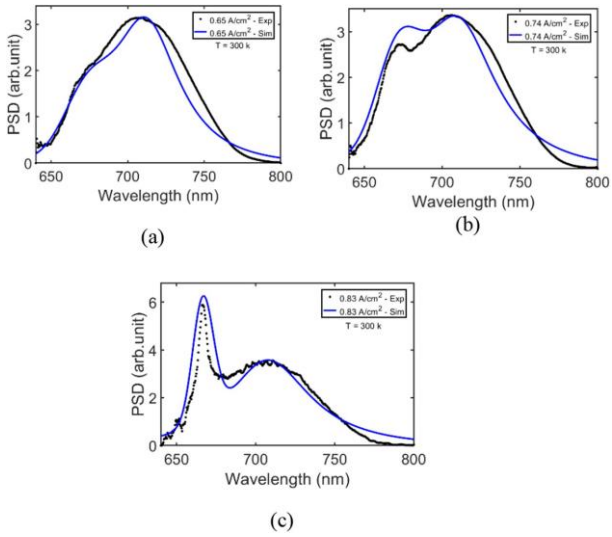

Figure 6 PSD in terms of wavelength for experimental data (dotted black) and simulation results (blue) at three different current densities.

4 Comparison of modeling results with experimental results

Research has shown that smaller quantum dots have only one bound energy level for electrons, while larger quantum dots have at least two levels. This leads to faster trapping times for larger quantum dots with significant ground state filling. As mentioned above, recombination occurs faster in small quantum dots due to stronger overlapping of wave functions, so the radiative lifetime for small quantum dots is set to smaller values than larger dots. Fig. (5) is used for the extracted spectral width and central wavelength values.

Figs (a6) to (c6) show the power spectral density in terms of wavelength obtained from model simulation and experimental data for three different average injection current densities. These figures show the transition between the three regions discussed earlier. The error percentage of the experimental and theoretical results is around 1.5 to 10%. Therefore, a good overall agreement was obtained between the theoretical and experimental results for different mean current densities.

5 Conclusion

This research presented the experimental and theoretical investigation of a double-layer quantum dot laser with the superposition of small and large quantum dots. Also, the dipole size distribution of quantum dots in InP lasers was presented for the first time. We showed that small quantum dots have the greatest effect on laser performance. they had. A two-peak Gaussian fitting model was applied to the data to extract the central emission wavelengths and the percentage contribution of small and large quantum dots in the emission. It is shown that small quantum dots dominate and emit lasers, while large quantum dots saturate. This is due to the higher mode gain of small quantum dots compared to larger dots. The theoretical model described this phenomenon as the superposition of two groups of heterogeneous quantum dots. The simulation results were compared with the experimental data, and the error percentage was obtained in the range of 1.5% to 10%, indicating a good agreement.

References

1. P. R. A. Abbas, H., Omran, Y. M.,Sabry; , 27th Intern. Semiconduct. Laser Conference (2021)
2. M. Asada, Y., Miyamoto, Y. Suematsu, IEEE J. Quantum Electron, **22** (1986)
3. G. J. Beirne, P. Michler, M. Jetter, H. Schweizer, J. Appl. Phys. (2005)
4. S. Breuer, M. Rossetti, L. Drzewietzki, P. Bardella, I. Montrosset, W. Elsaser, IEEE J. Quant. Elect. **47** (2011)
5. M. Califano, P. Harrison, Phys. Rev. B, **61** (2000)
6. N. Dogru, H. S. D. Tunc, et al. Opt. Laser Technol. **148** (2022)
7. J. F. Ehlert, A. Mugnier, G. He, F. GrillotLaser Phys. **31**, 8, (2021)
8. T. Finke, V. Sichkovskyi, J. P. Reithmaier, IEEE Photon. Technol. Lett. **33**, 14 (2021)
9. J. O. Gerguis, Y. M. Sabry, H. Omran, D. J. Khalil, J. Lightwave Technol. **37**, 20 (2019)
10. F. Grillot, K. Veselinov, M. Gioannini, I. Montrosset, J. Even, R. Piron, E. Homeyer, S. Loualiche, Quantum **45**, 7 (2009)
11. S. Grosse, J. Sandmann, G. von Plessen, J. Feldmann, H. Lipsanen, M. Sopanen, J. Tulkki, Phys. Rev. B **55**, 7 (1997)
12. I. S. Han, J. S. Kim, J. C. Shin, J. O. Kim, S. K. Noh, S. J. Lee, S. J. Krishna, Lumin. **207** (2019)
13. Z. Huang, S. Hepp, R. Sittig, M. Jetter, P. Michler, Optics InfoBase Conf. Pap. **140** (2009)
14. Z. Huang, M. Zimmer, S. Hepp, M. Jetter, P. Michler, IEEE J. Quantum Electron. **55**, 2 (2019)
15. S. M. Izadyar, M. Razaghi, A. Hassanzadeh, Opt. Quant. Electron. **50**, 1 (2018)
16. Z.F. Jiang, Z. M. Wu, E. Jayaprasath, W. Y. Yang, C. X. Hu, G. Q. Xia, Photonics **6**, 2 (2019)
17. A. V. Nenashev, A. V. Dvurechenskii, J. Appl. Phys. **10** (2020)
18. A. Quirce, M. Virte, *Nonlinear Dynamics of Semiconductor Lasers and Their Applications* (MDPI-Multidisciplinary Digital Publishing Institute, 2022)
19. J. Wang, F. Sciarrino, A. Laing, M. G. Thompson **14**, 5 (2020).
20. Y. Xiong, X. Zhang, J. Appl. Phys. **125**, 9 (2019)
21. Y. Zhang, L. Wang, K., Wang, K. S. Wong, K. Wu, IEEE Access **7**, 1 (2019).
22. Y. Zhou, J. Duan, F. Grillot, C. Wang, IEEE J. Quant. Electron (2020).